Sheet-crack cements in Marinoan (635 Ma) cap dolostones as regional benchmarks of vanishing ice-sheets.

Earth and Planetary Science Letters 300 (2010) 374–384

Contents lists available at ScienceDirect

Earth and Planetary Science Letters

journal homepage: www.elsevier.com/locate/epsl

Sheet-crack cements and early regression in Marinoan (635 Ma) cap dolostones: Regional benchmarks of vanishing ice-sheets?

Paul F. Hoffman [a,b,*], Francis A. Macdonald [a]

[a] Department of Earth and Planetary Sciences, Harvard University, 20 Oxford Street, Cambridge, MA, USA 02138
[b] School of Earth and Ocean Sciences, University of Victoria, Box 1700, Victoria, British Columbia, Canada V8W 2Y2

ARTICLE INFO

Article history:
Received 23 November 2009
Received in revised form 17 October 2010
Accepted 20 October 2010

Editor: M.L. Delaney

Keywords:
cap carbonate
sea-level
sheet-crack cement
pore-fluid overpressure
Marinoan glaciation
Namibia

ABSTRACT

Sheet-crack cements and coextensive intrastratal folds and breccias occur in a stratigraphically controlled, meter-thick zone, near the base of Marinoan (635 Ma) cap dolostones in slope settings. We demonstrate that sheet-crack cements on the margins of the Congo and Kalahari cratons are localized at a turbidite-to-grainstone transition, which records a transient fall in relative sea-level, preceding the larger glacioeustatic transgression. Sheet-cracks opened vertically, implying that pore-fluid pressure exceeded lithostatic pressure. When the margin of an ice-sheet retreats from a coast, a net fall in sea-level occurs in the vicinity, because of the weakened gravitational attraction between the ice-sheet and the nearby ocean. Augmented by glacioisostatic adjustment (postglacial rebound), the early regional fall in relative sea-level can mask the simultaneous rise in global mean sea-level caused by the addition of meltwater. We propose that sheet-cracks and related structures in Marinoan cap dolostones manifest pore-fluid overpressures resulting from rapid sea-level falls in the vicinity of vanishing ice-sheets.

1. Introduction

During the younger Cryogenian (Marinoan) glaciation, the continents were huddled between 30°N and 70°S latitude (Fig. 1). The 'Northern Ocean' would have dominated ocean circulation had it not been covered by perennial sea ice. Dynamic ice-sheets shrouded virtually every continent and many drained directly into the ocean, even along the palaeoequator (Evans, 2000, 2003; Evans and Raub, in press; Hambrey and Harland, 1981; Harland, 1964; Hoffman and Li, 2009; Trindade and Macouin, 2007). Whether a dynamic 'sea-glacier' fully covered the ocean, or large areas of seasonally open water persisted through the glacial maxima, is controversial (Goodman and Pierrehumbert, 2003; Hyde et al., 2000; Lewis et al., 2007; Liu and Peltier, 2010; Pollard and Kasting, 2005; Warren et al., 2002). Widespread geological evidence for dynamic (wet base) glaciation on land (Deynoux, 1985; Domack and Hoffman, in press; Dow and Gemuts, 1969; Edwards, 1984; Hambrey, 1982; Hambrey and Spencer, 1987; Hoffman, 2005; Kellerhals and Matter, 2003; McMechan, 2000) suggests that the ice-sheets were in dynamic steady state, broadly comparable to the present East Antarctic Ice Sheet (Donnadieu et al., 2003; Liu and Peltier, 2010; Pollard and Kasting, 2004). It has a mean thickness above sea-level of ~2.0 km (Lythe et al., 2001), and most of its interior area and outlet ice-streams undergo basal melting (Pattyn, 2010). Given the extent and thickness of Marinoan ice-sheets, the glacial ocean was ~25% smaller in volume, with a proportional increase in salinity, than when ice-sheets were absent. This corresponds to a difference in mean sea-level of ~1.0 km, insensitive to the contested differences in marine ice extent.

The abrupt termination of the Marinoan glaciation at 635 Ma (Condon et al., 2005) caused vast coastal flooding. Remarkably, meters to decameters of carbonate sediment, dubbed "cap dolostones", were draped across continental margins and marine platforms worldwide as flooding progressed (Bertrand-Sarfati et al., 1997; Font et al., 2010; Grotzinger and Knoll, 1995; Halverson et al., 2004; Hoffman and Li, 2009; Hoffman et al., 2007; James et al., 2001; Jiang et al., 2006; Kennedy, 1996; Nogueira et al., 2003; Rose and Maloof, 2010; Shields, 2005). They directly overlie terminal glacial deposits without evident hiatus, and they drape the sub-glacial erosion surface far beyond the confines of glacial deposits. They represent singular events: multiple cap dolostones are not observed, even where multiple "glacial–nonglacial" cycles are present (Allen et al., 2004; Rieu et al., 2007). Cap dolostones were deposited diachronously, from oldest to youngest with increasing palaeo-elevation. Their mass and extent connote an anomalous flux of alkalinity during deglaciation (Higgins and Schrag, 2003), in addition to strong surface warming and the disproportionate concentration of continents in low latitudes, where carbonate productivity is greatest. Systematic spatial and temporal variations in $\delta^{13}C$ (Halverson et al., 2004; Hoffman et al.,

* Corresponding author. 1216 Montrose Ave., Victoria, BC V8T 2K4, Canada. Tel.: +1 250 380 0059; fax: +1 250 592 5528.
E-mail address: paulfhoffman@yahoo.com (P.F. Hoffman).

0012-821X/$ – see front matter © 2010 Elsevier B.V. All rights reserved.
doi:10.1016/j.epsl.2010.10.027

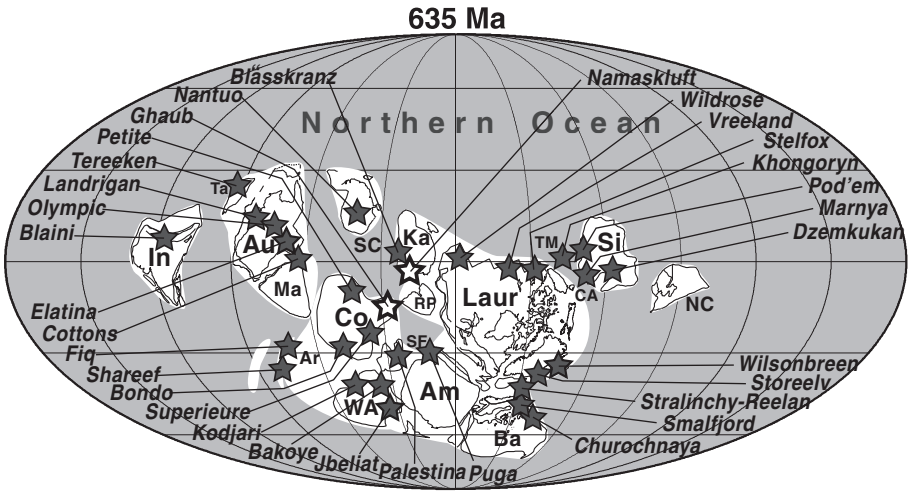

Fig. 1. Global palaeogeographic model for 635 Ma, constrained by palaeomagnetic data and chronotectonic 'bar-coding' (modified after Li et al., 2008; Hoffman and Li, 2009). Stars show the distribution of named late Cryogenian (Marinoan) glacigenic formations with cap dolostones. Open stars are the areas described in this paper. Palaeocontinents: Am, Amazonia; Ar, Arabia; Au, Australia; Ba, Baltica; CA, Chukotka-Arctic Alaska; Co, Congo; In, India; Ka, Kalahari; Laur, Laurentia including Rubia (Hildebrand, 2009); Ma, Mawson; NC, North China; RP, Rio Plata; SF, São Francisco; Si, Siberia; SC, South China; Ta, Tarim; TM, Tuva-Mongolia; WA, West Africa.

2007; James et al., 2001; Kennedy et al., 1998) demonstrate that cap dolostones were not detrital in origin, as does their occurrence in areas where sources of detrital carbonate were absent (Jiang et al., 2003; Nogueira et al., 2003). Marinoan cap dolostones are typically pale pinkish-grey (weathering to yellowish-grey) in colour and are extremely lean, containing less than 0.001 by weight of total organic carbon. Their conspicuous lamination is defined by normal and reverse graded micro- and macropeloids, deposited as hydraulically-sorted silt-, sand- and granule-size (<3.0 mm diameter) spherical aggregates (Aitken, 1991; Hoffman et al., 2007; James et al., 2001; Kennedy, 1996; Xiao et al., 2004). They were deposited mainly below sea-level and above prevailing wave base; inter- and supratidal indicators are uncommon except in specific regions (Shields et al., 2007; Zhou et al., 2010). Cap dolostones represent the transgressive tract of a global depositional sequence (Hoffman and Schrag, 2002) and, where fully developed, they grade upward into deeper water (below storm wave base) hemipelagic (limestone, marl and/or shale) rhythmite, representing the maximum of the postglacial flood.

Cap dolostones display idiosyncratic sedimentary features (Table 1) whose mutual stratigraphic relations are broadly consistent within and between cap dolostones in different regions (Allen and Hoffman, 2005; Hoffman et al., 2007). Here, we focus on one such structure, sheet-crack cements (Kennedy et al., 2001), which we observe to be consistently associated with an early fall in relative sea-level, preceding the major flood. We suggest that it is analogous to the rapid regression of early Holocene age in Greenland, which is attributed to the combined effects of glacial isostatic adjustments (rebound) and the weakening gravitational 'pull' on the adjacent ocean by the receding ice sheet (Clark, 1976). The gravitational effect is instantaneous, dictated by the rate and pattern of ice-sheet mass loss (Clark, 1976; Clark et al., 2002; Farrell and Clark, 1976; Tanner and Clark, 1976; Tapscott and Clark, 1976). The early Holocene regression in Greenland occurred later, relative to the 'glacioeustatic' rise in global mean sea-level, than the early regressions in Marinoan cap dolostones in Namibia. This is because the palaeotropical Congo and Kalahari cratons (Fig. 1) were among the first in the world to lose their ice-sheets (Hoffman and Li, 2009). The idea that regional sea-level must rise and fall, by tens of meters, in response to the waxing and waning of nearby ice-sheets is not new (Penck, 1882, cited in Jamieson, 1882).

First, we document the stratigraphic association of sheet-crack cements with early regression in Marinoan cap dolostones on the Congo and Kalahari cratons of Namibia. The sedimentary facies and pattern of $\delta^{13}C_{carb}$ variation in the Keilberg cap dolostone of the Otavi Group (Congo craton) has been described previously (Hoffman et al., 2007) and only a brief recap is needed. The Dreigratberg (new name) cap dolostone of the Port Nolloth Group in the Gariep Belt (Kalahari craton) is described here for the first time. It was previously correlated with the Bloeddrif Member of the Holgat Formation, which is the cap

Table 1
Sedimentary structures in Marinoan cap dolostones (top to bottom).

Sedimentary structure	Description	Preferred interpretation	Alternative interpretations
Sea-floor barite	Roseate clusters of bladed barite crystals in cm-scale digitate masses with internal growth laminae. Interspaces are filled by laminated peloidal ferroan dolomite, intermittently bridged by barite	Sulfate/ferrous boundary in the water column (Hoffman and Schrag, 2002)	Methane cold seepage (Jiang et al., 2006)
Giant wave ripples	Steep, highly aggradational megaripples with sharp, straight and parallel crestlines, and bidirectional laminae that intersect in the crestal region and coarsen crestward. Relief typically ~35 cm crest to trough; width ~150 cm crest to crest. Ripple sets aggrade sigmoidally for up to 140 cm and terminate through onlapping	Long-period waves (Allen and Hoffman, 2005)	Growth faulting (Gammon et al., 2005)
Tubestone stromatolite	Confluent, meter-scale, domal or corrugate stromatolites, hosting synsedimentary, cm-scale tubes, oriented palaeovertically (geoplumb), filled by meniscus laminated dolomicrite and/or void-filling cements	Gas or fluid escape (Cloud et al., 1974)	Organosedimentary growth form (Corsetti and Grotzinger, 2005)
Low-angle crossbedding	Laminated, normal and reverse graded, peloidal grainstone with meter-scale, low-angle toplaps, downlaps and onlaps	Storm waves (James et al., 2001)	Dissolution and flowage (Kennedy, 1996)
Sheet-crack cements	Bedding-parallel (rarely perpendicular) extension cracks, filled by fibrous, isopachous dolospar and locally late drusy quartz	Pore-fluid overpressures (Corkeron, 2007)	Methane cold seeps (Kennedy et al., 2001)

limestone above the older (Sturtian) Numees glacigenic diamictite (Frimmel, 2008). The description here complements and extends previous observations and correlations (Macdonald et al., in press). Finally, we speculate on a causal mechanism that links early regression with the development of sheet-crack cements in cap dolostones.

2. Sheet-crack cements and associated intrastratal folds

Sheet-cracks are planar openings, commonly buckled, that accommodate extension perpendicular, rarely parallel, to bedding. Their typical aspect ratio of ~0.02 (width/length) is supported by isopachous cement, precipitated as linings of constant-thickness, which are composed of fibrous dolomite oriented normal to the crack walls and local, late-stage, drusy quartz (Figs. 2a, b, 3a). Sheet-crack cements are characteristic of but not unique to Marinoan cap dolostones (Bertrand-Sarfati et al., 1997; Corkeron, 2007; Edwards, 1984; Hoffman et al., 2007; Jiang et al., 2006; Kennedy, 1996; Macdonald et al., in press; McCay et al., 2006; Nédélec et al., 2007; Plummer, 1978; Shields, 2005; Sumner, 2002), where they are typically confined to a meter-thick zone near the base of the cap dolostone (Corkeron, 2007; Kennedy, 1996; Kennedy et al., 2001). Volumetric expansion, both normal and parallel to bedding, is required to accommodate densely-developed sheet-crack cements. This is expressed in the form of variably-oriented intrastratal buckles and folds (Figs. 2a, b, 3a), the severity of which increases directly with the volumetric fraction of cement. The combination of intrastratal folds and isopachous cements invites comparison with peritidal 'tepee' structures (Assereto and Kendall, 1977), but sheet-crack cements in cap dolostones formed

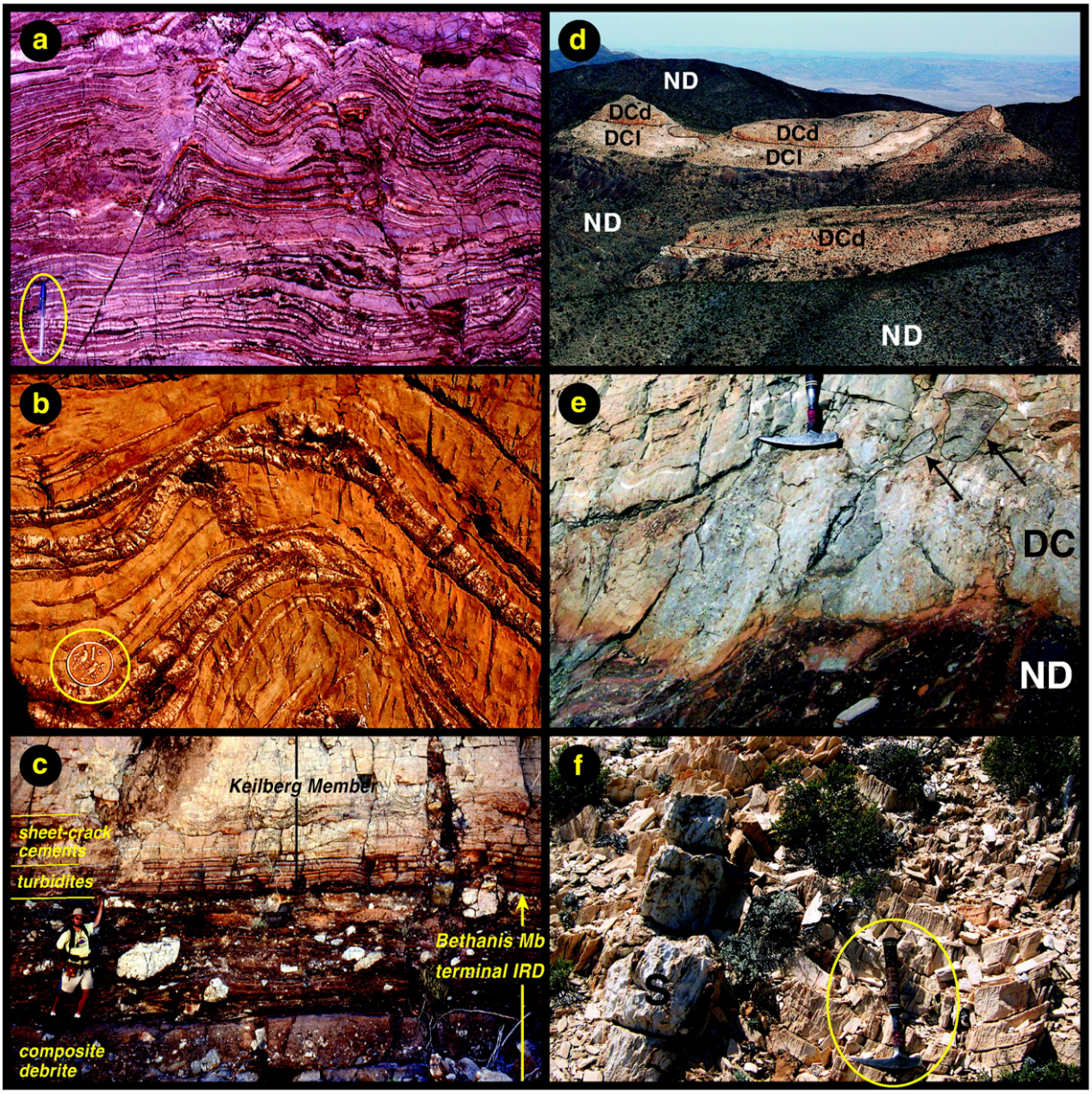

Fig. 2. Lithofacies of Marinoan (635 Ma) cap dolostones on the distal foreslope of the Otavi platform in northern Namibia (a–c) and on the western margin of the Kalahari craton in southern Namibia (d–f). (a) Sheet-crack cements composed of fibrous isopachous dolomite (white) and late drusy quartz (orange stain), with associated intrastratal folds, basal Keilberg cap dolostone, Garettes pos (section P6540). (b) Micropeloidal dolostone (yellow) with isopachous sheet-crack cements (white) at the crest of an intrastratal anticline, Fransfontein (section P7002). (c) Terminal Bethanis Member of the glacigenic Ghaub Formation, conformably overlain by basal turbidites and sheet-crack cements of the Keilberg cap dolostone, Narachaams se pos (section A, P1607, in Fig. 4). (d) Namaskluft diamictite (ND) overlain by channelized white limestone (DCl) and buff micropeloidal dolostone (DCd) of the Dreigratberg member, looking west from the top of the escarpment above Namaskluft Camp. (e) Clasts of Palaeoproterozoic basement rocks (arrows) at base of Dreigratberg member above Namaskluft Camp. Note also the sheet-crack cement and buckling of beds developed to the left of the hammer. (f) Giant wave ripples and elongate stromatolite (S) above Namaskluft Camp.

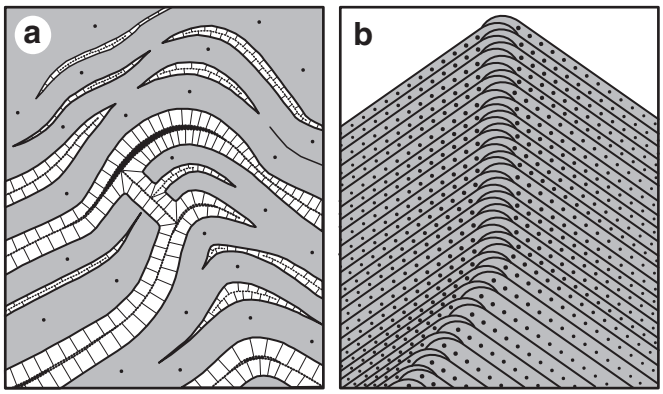

Fig. 3. Contrast between the crestal regions of (a) an intrastratal anticline associated with sheet-crack cements and (b) a giant wave ripple. Note the fibrous radiaxial dolosparite (clear) filling the folded sheet-cracks (a); and the interdigitation of opposing laminae, crestward-coarsening of peloids and strongly aggradational character of the wave ripple (b).

exclusively below a sediment–water interface (Corkeron, 2007; Kennedy, 1996; Kennedy et al., 2001), unlike 'tepee' structures which result from subaerial exposure and evaporative pumping (Assereto and Kendall, 1977; Kendall and Warren, 1987). Intrastratal folds associated with sheet-crack cements should also not be confused with giant wave ripples (Table 1), which lack void-filling cement and in which the laminae interdigitate in the crestal region (Fig. 3b) as a result of oscillatory traction across the ripple crest (Allen and Hoffman, 2005).

We are aware of only two explanations for sheet-crack cements in Marinoan cap dolostones. The first is that they represent cold seeps on the sea-floor, caused by flood-induced destabilization of permafrost hydrates presumed to have developed in organic-rich shelf sediments during the glacial sea-level lowstand (Jiang et al., 2003, 2006; Kennedy et al., 2001). The existence of permafrost assumes that the shelf was not well insulated by an ice sheet. One difficulty with this model is the extreme paucity of cement with very depleted $\delta^{13}C$ values (Jiang et al., 2003; Wang et al., 2008), which are diagnostic of modern and ancient cold seep carbonate cements (Kauffman et al., 1996; Michaelis et al., 2002). In the Keilberg cap dolostone of the Congo craton, the $\delta^{13}C$ and $\delta^{18}O$ values for isopachous cements and coexisting sediments are statistically indistinguishable (Supplementary Fig. S1). A second difficulty is the lateral continuity of the meter-thick zone of sheet-crack cements. We observed no discrete center in tens of kilometers of continuous outcrop section, nor are the underlying strata or the base of the cap dolostone disturbed as would be expected if methane had erupted from below (Hoffman et al., 2007). Taking a different approach, Corkeron (2007) attributes sheet-cracking and brecciation to pore-fluid overpressures, caused by rapid carbonate sedimentation and differential burial compaction of stratigraphically underlying mud, now shale. We are attracted to pore-fluid overpressures as a means of jacking open sheet-cracks, but place the ultimate cause of the overpressures elsewhere.

3. Otavi platform, Congo craton, northern Namibia

The Otavi Group is a 770–590 Ma carbonate platform exposed in the Damaran (590–530 Ma) Otavi fold belt, which rims the (present) southwestern promontory of the Congo craton. Two Cryogenian glaciations are represented in the Otavi Group, the older Chuos Formation and the *ca* 635 Ma Ghaub Formation (Halverson et al., 2005; Hoffman and Halverson, 2008; Hoffman et al., 1998; Hoffmann and Prave, 1996; Hoffmann et al., 2004;). The Ghaub Formation forms a marine ice grounding-zone wedge situated on the distal part of the south-facing foreslope of the Otavi platform (Domack and Hoffman, in press; Hoffman, 2005, 2010). Glacial deposits are absent on the upper foreslope and outer platform, 5 km seaward and 50 km landward of the slope break respectively, but a discontinuous veneer of lodgement tillite is found on the erosionally-deepened inner platform. A syndeglacial cap dolostone, the Keilberg Member of the Maieberg Formation (Hoffmann and Prave, 1996), conformably overlies the Ghaub Formation or the contiguous glacial erosion surface (Hoffman et al., 2007). The Keilberg Member (Fig. 4) is thicker on the upper

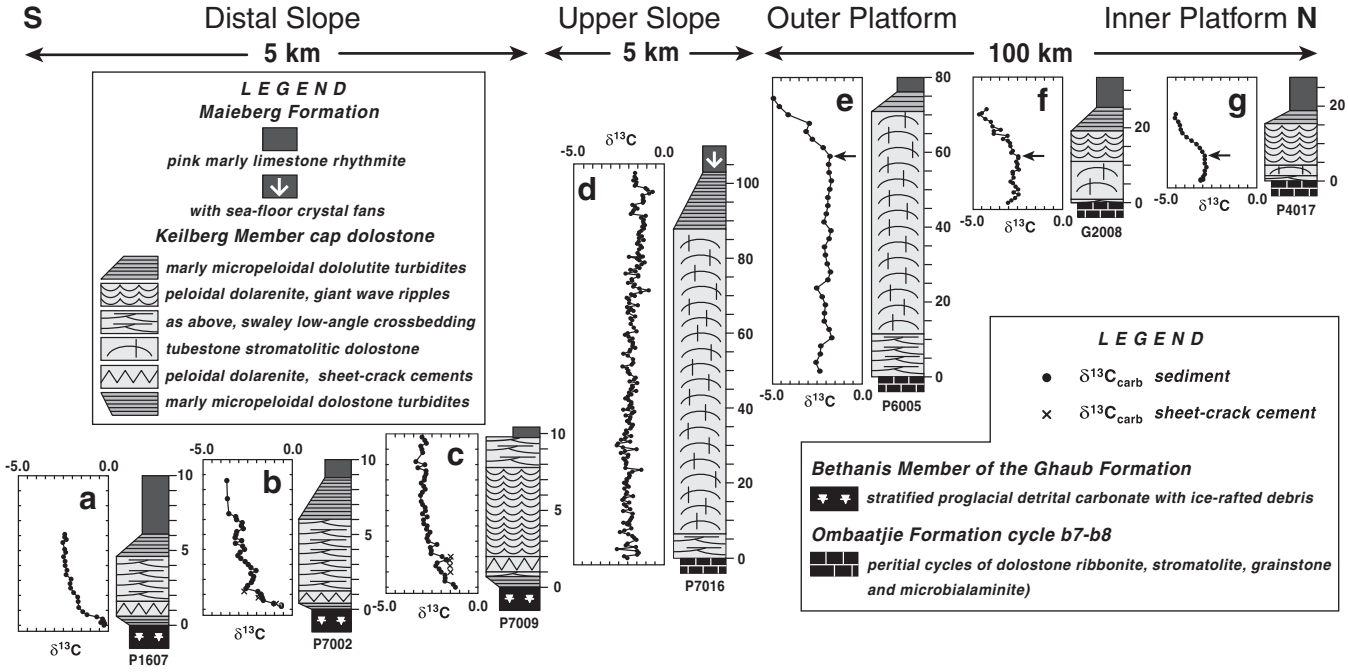

Fig. 4. Representative columnar sections with $\delta^{13}C_{dol}$ data of the Keilberg cap dolostone on the Otavi platform and its foreslope (modified after Hoffman et al., 2007). Columns are arranged vertically to fit a sigmoidal $\delta^{13}C$ profile with time progressing upward on the Y-axis. The steep initial decline in $\delta^{13}C$ is captured in sections a–c, the long slow rise in d–f, and the steep final decline in e–g (arrows at correlative inflections). Cap dolostone thickness variation controlled by tubestone stromatolite thickness. Greater thickness on the raised outer platform (e), compared with the depressed inner platform, indicates higher accumulation rates, not greater accommodation space. $\delta^{13}C$ and $\delta^{18}O$ values for sheet-crack cements and coexisting dolomicrite in sections a–c are plotted in Supplementary Fig. S1.

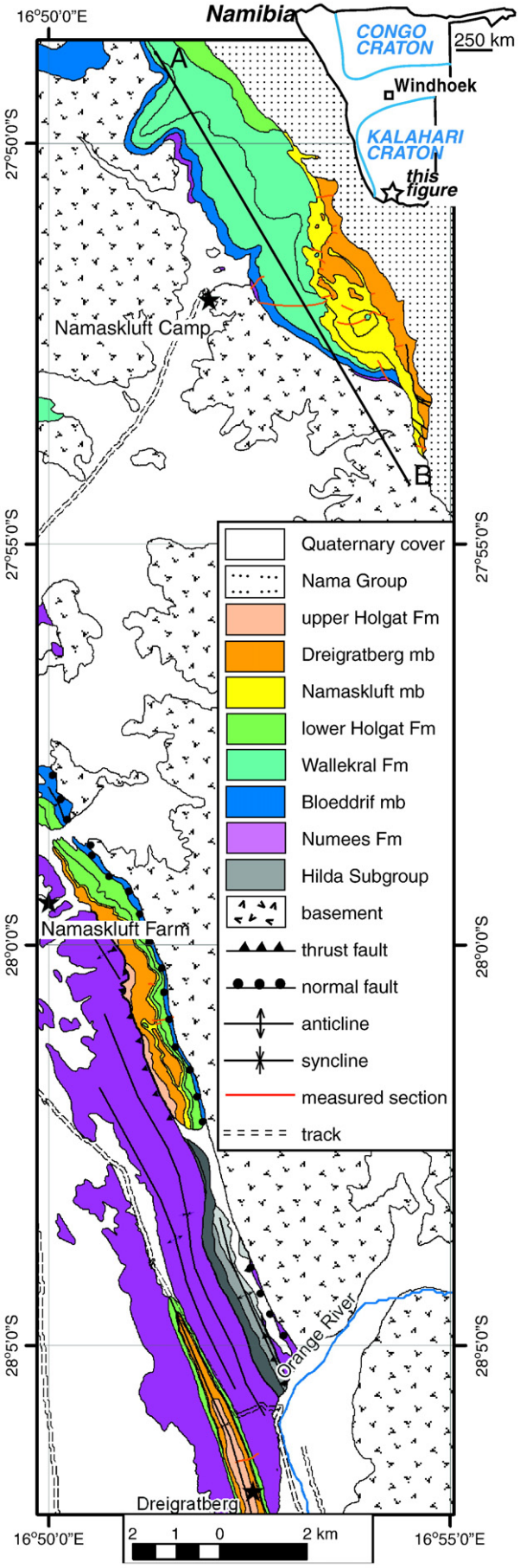

foreslope (<100 m) and outer platform (<75 m) where the Ghaub Formation is absent, and thinner on the inner platform (<25 m) and distal foreslope (<10 m). It forms the transgressive tract of the postglacial depositional sequence, the Maieberg Formation, and is everywhere conformably overlain by deeper water, marly limestone rhythmite of the maximum postglacial flood (Hoffman and Halverson, 2008; Hoffman and Schrag, 2002).

There are five basic carbonate lithofacies within the Keilberg cap dolostone (Fig. 4). All were deposited above prevailing wave base except for the carbonate turbidites, which mark the upper transition nearly everywhere and the base of the cap dolostone exclusively on the distal foreslope (Fig. 4). The regression (shoaling-upward transition) from basal turbidites into peloidal grainstone with low-angle cross-bedding is exceptional; it goes against the overall deepening-upward trend. The basal turbidites (Fig. 2c) are discrete, parallel-sided, graded units of dololutite, separated by shale partings. They thicken (0.5 to 2.0 cm), coarsen and amalgamate upward. The zone with sheet-crack cements consistently occurs directly above the turbidite-to-grainstone transition (Figs. 2c, 5). It is ~1.0 m thick and continues laterally for tens of kilometers parallel to depositional strike. Although spatially variable in the intensity of development, the cements do not form centered complexes, nor are the turbidites or the basal contact disturbed. The turbidites pinch out at the base of the upper foreslope, coincident with the disappearance sheet-crack cements (Fig. 4).

The question that emerges is, do sheet-crack cements systematically accompany regressive changes from basal turbidites to low-angle crossbedded grainstones? Kennedy (1996) documented a similar relationship in the lower part of the Marinoan cap dolostone in the Amadeus Basin of central Australia, but attributed the low-angle crossbedding (his Lithofacies II) to differential dissolution and semi-plastic slumping in a deepwater setting. We suggest that his graded, well-sorted macropeloids (Kennedy, 1996, Fig. 4b) accumulated above prevailing wave base. To further illustrate the coincidence of early regression and sheet-crack cements in cap dolostones, we next describe a new cap dolostone from a different craton in Namibia.

4. Gariep belt, Kalahari craton, southern Namibia

The Gariep belt is a Pan-African orogenic belt exposed on the western margin of the Kalahari craton in southwestern Namibia and northwestern South Africa (Stowe et al., 1984; Tankard et al., 1982). Folded strata in this late Ediacaran to Terraneuvian transpressional orogen (Davies and Coward, 1982) include the Port Nolloth Group (PNG), which formed as a consequence of rifting on the Kalahari margin of the Adamastor palaeocean (Frimmel, 2008), and the Nama Group, which was deposited in a foreland basin developed in response to collisions between the Kalahari, Congo and Rio de la Plata Cratons (Germs and Gresse, 1991; Gresse and Germs, 1993; Grotzinger and Miller, 2008; Grotzinger et al., 1995). The PNG contains a pre-Sturtian diamictite (Kaigas Formation) of uncertain origin, and discrete Sturtian (Numees Formation) and Marinoan (Namaskluft diamictite) glacigenic deposits (Macdonald et al., in press). The Namaskluft diamictite is capped by the Dreigratberg member of the Holgat Formation, which contains geochemical and sedimentological features characteristic of Marinoan (basal Ediacaran) cap dolostones. Below we compare proximal sections of the Dreigratberg member that show evidence for upward-shallowing, with more distal sections that contain sheet-crack cements.

4.1. Inner shelf sections at Namaskluft Camp

On the escarpment above Namaskluft Camp (Fig. 5), the PNG fills a ~12-km-wide and 1-km-deep palaeo-valley that is incised into

Fig. 5. Geological map of a part of the autochthonous (Namaskluft Camp) and parautochthonous (Namaskluft Farm and Dreigratberg) Port Nolloth Group on the eastern margin of the Gariep Belt in southern Namibia.

crystalline basement (Fig. 6). This panel is separated from more internal, parautochthonous sections by crystalline basement (Fig. 5).

The palaeo-valley at Namaskluft Camp was cut into an uplifted rift-shoulder during the Sturtian glaciation (Macdonald et al., in press). It is lined by Sturtian-age glacial deposits (Numees Formation) and largely filled by allodapic carbonate and siliciclastic turbidites (Wallekraal Formation), consisting predominantly of Bouma sequences Ta-b. During the Marinoan glaciation, a valley developed on the south-side of the palaeo-canyon, preferentially eroding the underlying sedimentary rocks (Fig. 6). The upper palaeo-valley is at least 3 km-wide and 200 m deep, with a cross-sectional morphology similar to Pleistocene sub-glacial tunnel valleys (Boyd et al., 1988; Van Dijke and Veldkamp, 1996). Tunnel valleys form under high glaciostatic pressures during rapid deglaciation (Van Dijke and Veldkamp, 1996). The lower stratified diamictite facies of the Namaskluft diamictite include plowed clasts, laminated muds with soft-sediment deformation of glacitectonic origin, graded sandstone with rare lonestones, and planar bedding passing upwards to aggradational ripples, characteristic of upper flow regime (Macdonald et al., in press). This facies assemblage is characteristic of Pleistocene tunnel valleys (Eyles and McCabe, 1989). The massive diamictite facies at the top of the Namaskluft diamictite are interpreted to reflect a rainout till formed at the termination of glaciation. The overlying Dreigratberg cap carbonate is also channelized with a <30-m thick package of limestone turbidite (Fig. 2d) present between the Namaskluft diamictite and the cap dolostone (Fig. 7). This limestone body pinches out laterally and is succeeded by the buff-coloured dolostones of the Dreigratberg member, which contains giant wave ripples and tubestone stromatolites.

Fifteen detailed stratigraphic sections were measured through the Dreigratberg cap carbonate along the escarpment above Namaskluft Camp to track facies changes in a three dimensional framework (Fig. 7). Deposition begins with a channelized body of white to violet allodapic limestone with reduction spots (Fig. 2d) and shallows up to a fine-laminated micropeloidal dolomite with low-angle crossbedding. The limestone beds are graded and also contain thin green marl partings. Within 5 km to the northwest of its greatest thickness, the limestone turbidite interval thins to less than a meter. Cobble-sized lonestones of metamorphic basement and carbonate are present in these thin turbidite beds on the margin of the channel (Fig. 2e), but were not found in the thickest bodies of the basal Dreigratberg limestone.

The limestone turbidites are succeeded gradationally by fine-laminated, buff-coloured, micropeloidal dolostone with low-angle crossbedding. Sheet-crack cements occur near the base of the dolostone (Fig. 2e), but are poorly developed and laterally discontinuous. Within 2 m of the base of the dolostone, giant wave ripples form off of planar surfaces. Wave ripples near the base of the dolomite have <30 cm of synoptic relief and wavelengths >2 m (Fig. 2f). Elongate stromatolites appear ~2 m higher in the section, preferentially nucleated on the crests of the giant wave ripples. Microbialites become more dominant upwards and modify the size of the wave ripples, decreasing their wavelength and regularity (Fig. 2f). Throughout the cap dolostone, both the wave ripples and the elongate stromatolites maintain a consistent orientation ~100° azimuth. Some of the wave ripples are refolded, but the orientation of these later tectonic folds is ~158° azimuth, distinct from the orientation of the elongate stromatolites and wave ripples. Higher in the section, the elongate stromatolites coalesce to form a massive bioherms with tubestone structures (Corsetti and Grotzinger, 2005; Macdonald et al., in press). The bioherms are flooded by <300 m of pink to light grey allodapic limestone and siltstone with hummocky cross-stratification (upper Holgat Formation), variably truncated by the sub-Nama unconformity (Fig. 6).

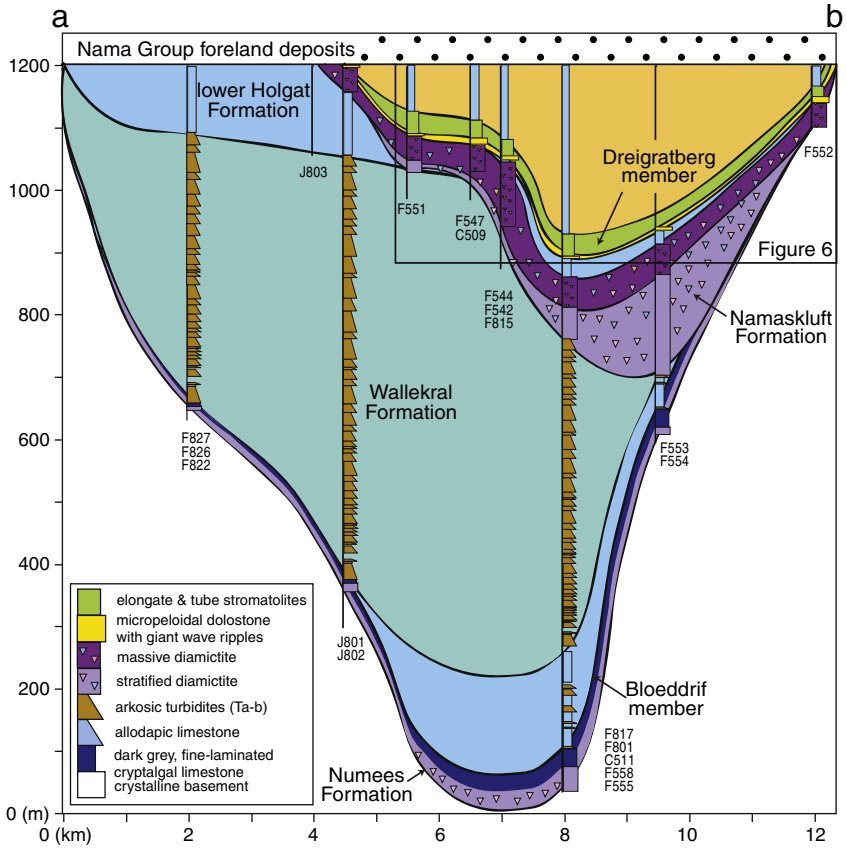

Fig. 6. Longitudinal (strike-parallel) cross-section of the escarpment above Namaskluft Camp. Line of cross-section shown in Fig. 1. Datum is the base of the Nama Group, a surface that certainly had some relief.

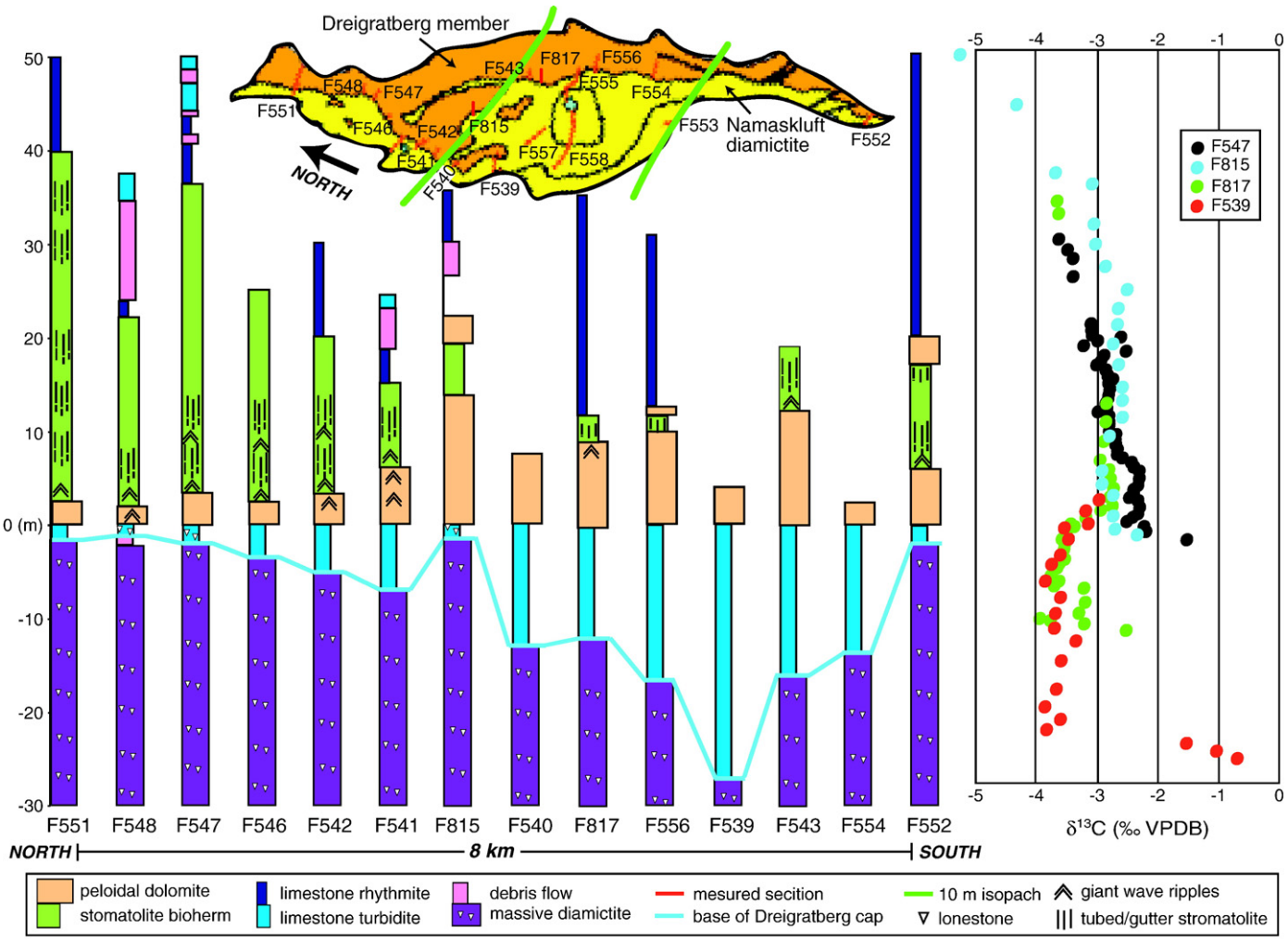

Fig. 7. Litho- and chemostratigraphy of the Dreigratberg cap carbonate in a longitudinal cross-section of the escarpment above Namaskluft Camp. Datum is the base of the cap dolostone.

4.2. Upper slope sections at Namaskluft Farm

The sections at Namaskluft Camp are separated from those at Namaskluft Farm by a basement high (Fig. 5). Along the southernmost exposures at Namaskluft Camp, the cap dolostone rests on basement, suggesting that this basement high persisted during deposition of the Dreigratberg member. At Namaskluft Farm, the Namaskluft diamictite is succeeded by less than a meter of green marl, a couple of meters of thin-laminated peloidal dolomite, then >30 m of massive stromatolite bioherm with irregular cements (Fig. 8). This is overlain by an ~50 m thick transgressive sequence of folded pink limestone rhythmite and an additional ~50 m of mixed allodapic carbonate and siliciclastic rocks of the upper Holgat Formation.

4.3. Distal sections at Dreigratberg

In deeper water sections ~20 km to the southwest of Namaskluft Camp at Dreigratberg, the Neoproterozoic stratigraphy is very condensed and consists predominantly of allodapic carbonate and argillite (Fig. 8). The Namaskluft diamictite is stratified and contains rare, subrounded carbonate and sandstone cobble dropstones that pierce the siltstone matrix lamination. The diamictite is sharply capped by 1.6 m of graded beds of allodapic limestone, which weathers white but is blue when fresh. These beds are interpreted as turbidites. They are succeeded by 0.4 m of dolostone with cements that are parallel to sedimentary bedding and buckled upwards into pseudo-tepees. These sheet-crack cements are isopachous, fibrous, and consist of dolospar. Unlike the giant wave ripples, the pseudo-teepee structures associated with the sheet-crack cements show no preferred orientation. The Dreigratberg member continues upwards with an additional ~50 m of pink limestone, characteristic of the upper portion of the Dreigratberg cap carbonate.

Sheet-crack cements are also present in distal sections of the Dreigratberg member in the Dolomite Peaks area of South Africa (Macdonald et al., in press).

4.4. Chemostratigraphy

Samples were collected from measured stratigraphic sections for $\delta^{13}C$ and $\delta^{18}O$ analyses. They were processed and analyzed using standard laboratory procedures (described in detail in Halverson et al., 2004).

The Dreigratberg member at Namaskluft Camp, Namaskluft Farm, and Dreigratberg all display $\delta^{13}C$ profiles with values beginning near −1‰, decreasing sharply in the lower couple of meters, and then increasing upwards through the most of the cap dolostone before plunging to the most depleted values at the top (Fig. 8). Values of $\delta^{13}C$ at Namaskluft Farm are consistently offset by ~+1‰ from those at Namaskluft Camp (Fig. 8).

4.5. Base-level fall

The Neoproterozoic palaeotopography on the escarpment above Namaskluft Camp affords a unique window into the relationship

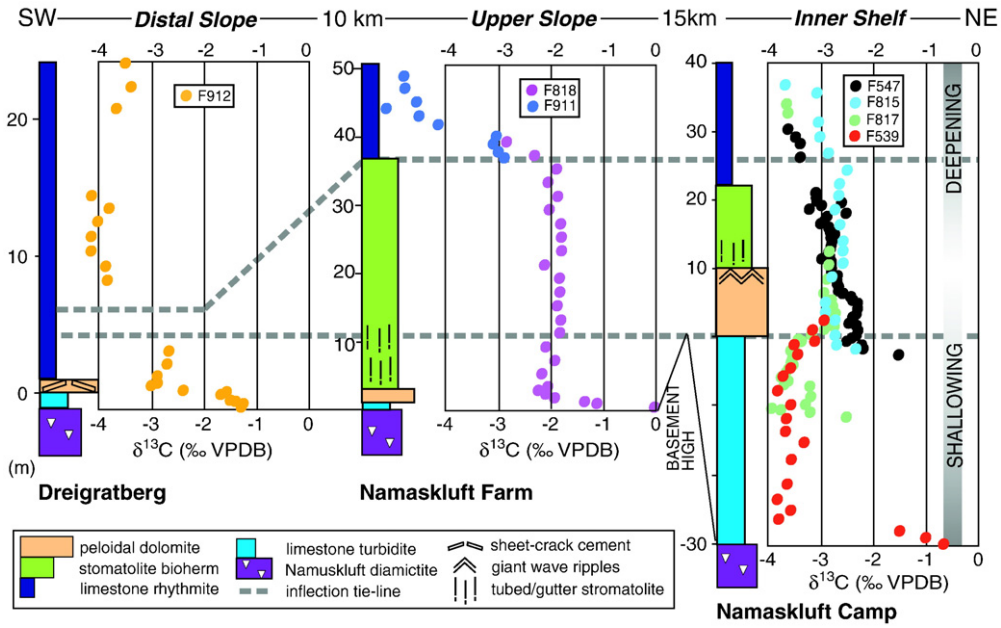

Fig. 8. Litho- and chemostratigraphies of the Dreigratberg cap carbonate in an oblique transverse cross-section from Dreigratberg to Namaskluft Camp (see Fig. 1 for locations). Columnar section at Namaskluft Camp is a cartoon section with the thickness of the basal turbidites from F539 and the thicknesses of the cap dolostone facies averaged from the sections shown in Fig. 6.

between base-level and facies change. Typically, the sedimentary facies of the Marinoan cap dolostone are in a characteristic order, progressing in a transgressive sequence up-section from a micropeloidal dolomite with low-angle crossbedding, to tubestone stromatolites, to giant wave ripples, and culminating with crystal fans precipitated at a dolomite–limestone transition (Hoffman et al., 2007), although one or more of these features are commonly missing from any individual outcrop. However, unlike cap carbonates elsewhere, along the escarpment, a channelized body of allodapic limestone is at the base, and is succeeded by a micropeloidal dolostone. The limestone hosts rare ice-rafted debris, marking the retreat of the ice-line. Within the overlying dolostone, giant wave ripples are always below or interbedded with elongate gutter stromatolites that progress upwards to tubestone stromatolites. Elongate stromatolites grow preferentially on the crests of giant wave ripples and coalesce upwards to form tubestone stromatolites. These facies patterns describe a high-stand tract prior to a transgression, and the characteristic sequence of sedimentary structures is inverted.

Carbon isotope chemostratigraphy suggests that the high-stand tract on the escarpment can be correlated with the condensed section at Dreigratberg. That is, the progression from channelized limestone turbidite to giant wave ripples and tubestone stromatolites on the escarpment is equivalent to the condensed turbidite to sheet-crack cement succession at Dreigratberg, both recording a fall in relative sea-level prior to the maximum flood at the top of the Dreigratberg member.

5. Discussion

5.1. Variable expressions of early regression

There are significant differences as well as obvious similarities between the Dreigratberg cap dolostone and its equivalent on the Otavi platform, the Keilberg Member (Figs. 4 and 8). In both areas, the cap dolostone is thinnest on the distal slope, thickest on the upper slope, and intermediate in thickness on the platform. In both areas, it features an overall sigmoidal $\delta^{13}C$ profile composed of three stages—a steep early decline, a long gradual rise, and a steep final descent. In both areas, $\delta^{13}C$ values through the gradual rise are consistently higher on the slope than on the inner shelf/platform. And in both areas, rifting had been active before, during and after the Sturtian glaciation, but the Marinoan glaciation encountered young passive margins undergoing regional subsidence of presumed thermal origin (Halverson et al., 2002; Macdonald et al., in press).

Hoffman et al. (2007) demonstrated that the Keilberg Member was strictly deposited within the flooding stage associated with global ice-sheet meltdown. On the assumption that this occurred rapidly because of positive climate feedbacks (e.g., ice-elevation, ice-albedo and greenhouse-gas feedbacks), they concluded that the observed change in $\delta^{13}C$ of >4‰ was far too large to reflect change in the isotopic composition of seawater, given the long residence time of C in seawater (100 s of kyrs) with elevated atmospheric pCO_2 (Bao et al., 2008). They postulated that the changes in $\delta^{13}C$ reflect a dominant role for temperature-dependent CO_2 (gas)–CO_3^{2-} isotopic fractionation at low pH (<7.2). Accordingly, the overall upward decline in $\delta^{13}C$ reflects strong warming as ice-sheets receded, lowering the planetary albedo by 0.3 (snowball Earth deglaciation). With insolation reduced by 6% relative to present, the albedo change amounts to a radiative forcing of nearly 100 W m^{-2}, of which ~11 W m^2 would be taken up in melting the global ice-sheets (Wallace and Hobbs, 1977, p. 320). Lower $\delta^{13}C$ values on the inner platform reflect warmer waters there during the gradual rise, compared to the slope. This reasoning may also apply to the Gariep belt, although the estimated horizontal temperature gradient across the Otavi platform of 0.1 °C km^{-1} (Hoffman et al., 2007) must have been <10× steeper to account for the telescoping of distance (Fig. 8). Alternatively, the lateral gradient could be a product of an isotopically-light carbon flux from the continent. Either way, we postulate that this gradient was maintained in part by a palaeotopographic basement high between the inner shelf and upper slope, above which the tubestone stromatolite of the Dreigratberg member was best developed, restricting circulation between the inner shelf and the open ocean.

Of the differences, four stand out. First, stratigraphic and isotopic variability is more localized in the Gariep belt. Changes that take place in 15 km across strike in the Gariep belt occur in 150 km across the Otavi platform (Figs. 4 and 8). This reflects more localized palaeotopography as discussed above. Second, compared with the Keilberg Member, the Dreigratberg sections are displaced 'downward', relative

to the sigmoidal $\delta^{13}C$ profile. The early steep decline is captured in all three sections in the Gariep belt but only on the distal foreslope of the Otavi platform (Figs. 4 and 8). The final steep descent is recorded in dolostone in all sections on the Otavi platform, but in the Gariep belt it only occurs in the limestone above the Dreigratberg member. This means that the Dreigratberg member began and ended earlier than the Keilberg Member, relative to the warming trend and the glacioeustatic rise. A simple explanation is that the Dreigratberg preserves the shoalwater depositional record at a lower mean palaeo-elevation than the Keilberg, thereby capturing an earlier phase of the glacioeustatic flood. Third, the early regression recorded in the Dreigratberg member extends over a thicker stratigraphic interval compared with the Keilberg Member. The regressive segment is <1.0 m thick in the Keilberg (Fig. 2c) but up to 40 m thick in the Dreigratberg member (Fig. 8). This is consistent with the Dreigratberg cap being slightly older than the Keilberg, which only caught the tail end of the early regression in its oldest sections (distal foreslope). And fourth, the early regression occupies only part of the initial steep decline in $\delta^{13}C$ in the Keilberg Member, but outlasts it in the Dreigratberg member (Figs. 4 and 8). This implies that relative sea-level continued to fall in the Gariep belt after it had stopped falling around the Otavi platform, assuming that the warming of surface waters (governing the $\delta^{13}C$ trajectory according to Hoffman et al., 2007) occurred simultaneously in both areas.

5.2. Early regression and sheet-crack cements

Why are sheet-crack cements closely associated with early regression? Before they were buckled, sheet-cracks opened vertically, parallel to the fibres of the cement, and against the force of gravity. This implies that pore-fluid pressure (pore pressure) exceeded the lithostatic pressure. When sedimentation occurs, the sediment acquires a pore pressure equal to the hydrostatic pressure. With burial, pore pressures increase on a trajectory intermediate between the hydrostatic and lithostatic pressure gradients (Fig. 9). This is referred to as pore-fluid overpressure. Overpressure allows sheet-cracks to form within the sediment. We propose that regionalized sea-level falls associated with the disappearance of ice-sheets lowered lithostatic pressures below the ambient pore pressure at shallow depths beneath the sediment–water interface (Fig. 9). Hydrostatic and lithostatic pressures drop by ~1 bar for every 10 m fall in sea-level. For this mechanism to be viable, the rate of sea-level fall must be rapid relative to the rate at which the sediment can depressurize by pore-fluid escape. Rapid cementation, which lowers permeability while increasing pore pressure, is an essential part of the proposed mechanism. The isopachous cements themselves provide undeniable evidence for rapid carbonate precipitation from pore waters synchronous with incremental sheet-crack opening. We discount remineralization of organic matter or methane hydrate as a driving force for overpressure because the $\delta^{13}C$ of the sheet-crack cement provides no support for an isotopically-light source of alkalinity (Supplementary Fig. S1). Our proposal provides a causal mechanism for the observed correlation of sheet-crack cements and early regression within cap dolostones.

5.3. Early regression and ice-sheet mass loss

What caused the early fall in relative sea-level? When a grounded ice-sheet forms near a coast, sea-level in its vicinity rises due to mutual gravitational attraction between the ice-sheet and the adjacent waters. At a glacial termination, sea-level in the vicinity of a melting ice-sheet will fall at a rate determined by the rate and distribution of ice-sheet mass loss (Clark, 1976; Farrell and Clark, 1976). The fall will be fastest where mass loss is concentrated at the periphery of an ice-sheet, causing the ice edge to retreat. By raising the land surface, glacioisostatic adjustments (GIA) also contribute to

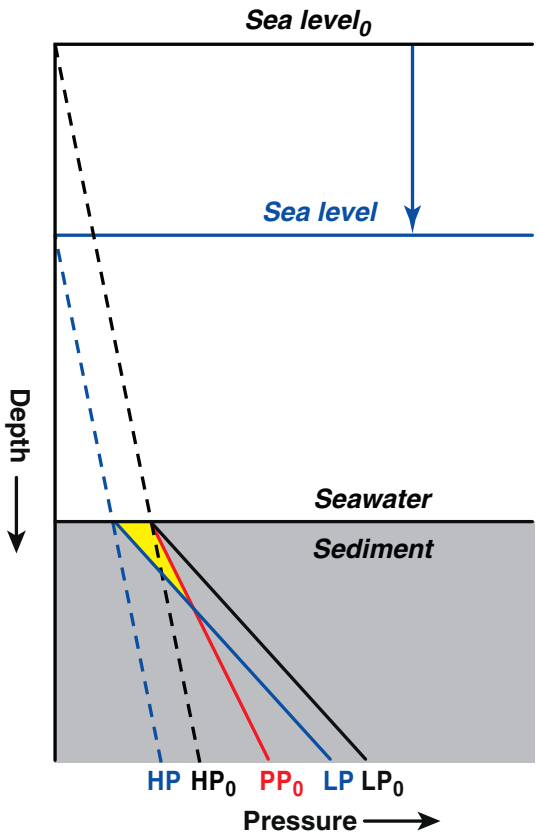

Fig. 9. Lithostatic pressures before (LP_0) and after (LP) after a sea-level fall, and their relation to equivalent hydrostatic pressures (HP_0 and HP) and the initial pore pressure (PP_0). The triangular area in yellow indicates the field where pore pressures potentially exceed lithostatic pressures after the sea-level fall, provided the fall is rapid relative to the rate at which the sediment will depressurize. Note that sedimentation during sea-level fall would not increase LP relative to PP_0: they would rise in unison.

early regression but, as the time-scale for GIA is more prolonged than the recession of the Laurentide and Scandinavian ice-sheets, Marinoan GIA has been identified with 'late regression', at the stratigraphic tops of cap dolostones (Bertrand-Sarfati et al., 1997; James et al., 2001; Nogueira et al., 2003; Shields et al., 2007; Zhou et al., 2010). We propose that early regressions in Marinoan cap dolostones in central Australia (Kennedy, 1996) and on the Congo and Kalahari cratons, are primarily related to the instantaneous gravitational effect on regional sea-level of ice sheet mass loss, complemented by GIA.

How fast did Marinoan ice-sheets vanish? From a climate physics perspective, it is generally assumed that Marinoan deglaciation was very rapid (a few kys) because of the preponderance of ice-sheets at low palaeolatitudes (Fig. 1), combined with extreme atmospheric pCO_2 (Bao et al., 2008, 2009). In contrast, the existence of apparent geomagnetic excursions and reversals in cap dolostones implies a time-scale of tens to hundreds of kyrs if Marinoan geomagnetic field behavior was similar to the Cenozoic (Font et al., 2010; Raub and Evans, 2006; Trindade et al., 2003). This conflict remains unresolved, but we find the shorter time-scale more compatible with the sedimentology of cap dolostones (Table 1). If Marinoan ice-sheets were buttressed by ice-shelves or a continuous 'sea-glacier' (Goodman and Pierrehumbert, 2003; Pollard and Kasting, 2005; Warren et al., 2002), their removal would have triggered rapid ice-sheet drainage, as observed in modern outlet glaciers when confined ice-shelves are lost (De Angelis and Skvarca, 2003). The sea-glacier would be lost before the ice-sheet because it is thinner and has a lower surface elevation. Because the rise in global mean sea-level due to the melting of Marinoan ice-sheets globally was roughly ten times larger than the regional fall in relative sea-level due to the gravitational effect of local

ice-sheet mass loss, ice-sheets must have vanished in sequence, not in unison, for the gravitational effect to reverse, not merely reduce, the rate of syndeglacial flooding.

6. Conclusions

Sheet-crack cements and associated intrastratal folds and breccias consistently follow regressive (shoaling-upward) intervals near the base of otherwise transgressive (deepening-upward) cap dolostones of earliest Ediacaran (Marinoan) age on the Congo and Kalahari cratons of Namibia. We relate the early regression to sea-level fall in the vicinity of an ice-sheet, as a gravitational response to its mass loss, complemented by glacial isostatic adjustment (postglacial rebound). The fall in relative sea-level, if rapid, could result in pore-fluid overpressures at shallow depths within sediment of low permeability, which we suggest as the mechanism for sheet-crack development. This would account for the stratigraphic association of sheet-crack cements with early regressions in Marinoan cap dolostones. If our model has merit, sheet-crack cements will be found to follow early regressions within Marinoan cap dolostones in other areas.

Supplementary materials related to this article can be found online at doi: 10.1016/j.epsl.2010.10.027.

Acknowledgements

Field work in Namibia was supported by the U.S. National Science Foundation grant EAR-0417422 (to PFH), the Earth System Evolution Program of CIFAR (Canadian Institute for Advanced Research), the Harvard University Center for the Environment (HUCE), and the Geological Survey of Namibia. Catherine Rose and Justin Strauss assisted in the field. Stable isotope measurements were made by Greg Eischeid in the Geochemical Oceanography Lab at Harvard. We are endebted to lab Director Dan Schrag for support and encouragement. We thank Peggy Delaney and an anonymous reviewer for helpful comments on the original manuscript.

References

Aitken, J.D., 1991. The Ice Brook Formation and post-Rapitan, late Proterozoic glaciation, Mackenzie Mountains, Northwest Territories. Geol. Surv. Can. Bull. 404 43 pp.
Allen, P.A., Hoffman, P.F., 2005. Extreme winds and waves in the aftermath of a Neoproterozoic glaciation. Nature 433, 123–127.
Allen, P., Leather, J., Brasier, M.D., 2004. The Neoproterozoic Fiq glaciation and its aftermath, Huqf Supergroup of Oman. Basin Res. 16, 507–534.
Assereto, R.L.A.M., Kendall CG, St. C, 1977. Nature, origin and classification of peritidal tepee structures and related breccias. Sedimentology 24, 153–210.
Bao, H., Lyons, J.R., Zhou, C., 2008. Triple oxygen isotope evidence for elevated CO_2 levels after a Neoproterozoic glaciation. Nature 452, 504–506.
Bao, H., Fairchild, I.J., Wynn, P.M., Spötl, C., 2009. Stretching the envelope of past surface environments: Neoproterozoic glacial lakes from Svalbard. Science 323, 119–122.
Bertrand-Sarfati, J., Flicoteaux, R., Moussine-Pouchkine, A., Aït Kaci Ahmed, A., 1997. Lower Cambrian apatitic stromatolites and phospharenites related to the glacio-eustatic cratonic rebound (Sahara, Algeria). J. Sed. Res. 67, 957–974.
Boyd, R., Scott, D.B., Douma, M., 1988. Glacial tunnel valleys and Quaternary history of the outer Scotian shelf. Nature 333, 61–64.
Clark, J.A., 1976. Greenland's rapid postglacial emergence: a result of ice–water gravitational attraction. Geology 4, 310–312.
Clark, P.U., Mitrovica, J.X., Milne, G.A., Tamisiea, M.E., 2002. Sea-level fingerprinting as a direct test for the source of global meltwater pulse 1A. Science 295, 2438–2441.
Cloud, P., Wright, L.A., Williams, E.G., Diehl, P., Walter, M.R., 1974. Giant stromatolites and associated vertical tubes from the upper Proterozoic Noonday Dolomite, Death Valley region, eastern California. Geol. Soc. Am. Bull. 85, 1869–1882.
Condon, D., Zhu, M., Bowring, S.A., Wang, W., Yang, A., Jin, Y., 2005. U–Pb ages from the Neoproterozoic Doushantuo Formation, China. Science 308, 95–98.
Corkeron, M., 2007. 'Cap carbonates' and Neoproterozoic glacigenic successions from the Kimberley region, north-west Australia. Sedimentology 54, 871–903.
Corsetti, F.A., Grotzinger, J.P., 2005. Origin and significance of tube structures in Neoproterozoic post-glacial cap carbonates: example from Noonday Dolomite, Death Valley, United States. Palaios 20, 348–363.
Davies, C., Coward, M.P., 1982. The structural evolution of the Gariep Arc in southern Namibia. Precambrian Res. 17, 173–198.
De Angelis, H., Skvarca, P., 2003. Glacier surge after ice shelf collapse. Science 299, 1560–1562.
Deynoux, M., 1985. Terrestrial or waterlain glacial diamictites? Three case studies from the late Proterozoic and late Ordovician glacial drifts in West Africa. Palaeogeogr. Palaeoclimatol. Palaeoecol. 51, 97–141.
Domack. E.W., Hoffman, P.F., in press. An ice grounding-line wedge from the Ghaub glaciation (635 Ma) on the distal foreslope of the Otavi carbonate platform, Namibia, and its bearing on the snowball Earth hypothesis. Geol. Soc. Am. Bull.
Donnadieu, Y., Fluteau, F., Ramstein, G., Ritz, C., Besse, J., 2003. Is there a conflict between the Neoproterozoic glacial deposits and the snowball Earth interpretation: an improved understanding with numerical modeling. Earth Planet. Sci. Lett. 208, 101–112.
Dow, D.B., Gemuts, I., 1969. Geology of the Kimberley Region, Western Australia. Bur. Min. Res. Geol. Geophys. Bull. 106 Canberra, ACT, 135 pp.
Edwards, M.B., 1984. Sedimentology of the Upper Proterozoic glacial record, Vestertana Group, Finnmark, North Norway. Nor. Geol. Unders. Bull. 394 76 pp.
Evans, D.A.D., 2000. Stratigraphic, geochronological, and paleomagnetic constraints upon the Neoproterozoic climatic paradox. Am. J. Sci. 300, 347–433.
Evans, D.A.D., 2003. A fundamental Precambrian–Phanerozoic shift in earth's glacial style? Tectonophysics 375, 353–385.
Evans, D.A.D., Raub, T.D., in press. Neoproterozoic glacial palaeolatitudes: a global update. In: The Geological Record of Neoproterozoic Glaciations (E. Arnaud, G.P. Halverson and G. Shields, eds), Geol. Soc. London Spec. Publ.
Eyles, N., McCabe, A.M., 1989. Glaciomarine facies within subglacial tunnel valleys: the sedimentary rerocrd of glacio-isostatic downwarping in the Irish Sea Basin. Sedimentology 36, 431–448.
Farrell, W.E., Clark, J.A., 1976. On postglacial sea level. Geophys. J. R. Astr. Soc. 46, 647–667.
Font, E., Nédélec, A., Trindade, R.I.F., Moreau, C., 2010. Fast or slow melting of the Marinoan snowball Earth? The cap dolostone record. Palaeogeogr. Palaeoclimatol. Palaeoecol. 295, 215–225.
Frimmel, H.E., 2008. Neoproterozoic Gariep Orogen. In: Miller, R.McG. (Ed.), The Geology of Namibia, Neoproterozoic to Lower Palaeozoic, vol. 2. Geological Survey of Namibia, Windhoek. 14-0–14-39.
Gammon, P.R., McKirdy, D.M., Smith, H.D., 2005. The timing and environment of tepee formation in a Marinoan cap carbonate. Sed. Geol. 177, 195–208.
Germs, G.J.B., Gresse, P.G., 1991. The foreland basin of the Damara and Gariep Orogens in Namaqualand and southern Namibia: stratigraphic correlations and basin dynamics. S. Afr. J. Geol. 94, 159–169.
Goodman, J., Pierrehumbert, R.T., 2003. Glacial flow of floating marine ice in "Snowball Earth". J. Geophys. Res. 108. doi:10.1029/2002JC001471.
Gresse, P.G., Germs, G.J.B., 1993. The Nama foreland basin: sedimentation, major unconformity bounded sequences and multisided active margin advance. Precambrian Res. 63, 247–272.
Grotzinger, J.P., Knoll, A.H., 1995. Anomalous carbonate precipitates: is the Precambrian the key to the Permian? Palaiyos 10, 578–596.
Grotzinger, J.P., Miller, R.McG., 2008. Nama Group. In: Miller, R.McG. (Ed.), The Geology of Namibia, Neoproterozoic to Lower Palaeozoic, vol. 2. Geological Survey of Namibia, Windhoek. 13-229–13-272.
Grotzinger, J.P., Bowring, S.A., Saylor, B.Z., Kaufman, A.J., 1995. Biostratigraphic and geochronologic constraints on early animal evolution. Science 270, 598–604.
Halverson, G.P., Hoffman, P.F., Schrag, D.P., Kaufman, A.J., 2002. A major perturbation of the carbon cycle before the Ghaub glaciation (Neoproterozoic) in Namibia: Prelude to snowball Earth? Geophys. Geochem. Geosystems 3. doi:10.1029/2001GC000244.
Halverson, G.P., Maloof, A.C., Hoffman, P.F., 2004. The Marinoan glaciation (Neoproterozoic) in northeast Svalbard. Basin Res. 16, 297–324.
Halverson, G.P., Hoffman, P.F., Schrag, D.P., Maloof, A.C., Rice, A.H.N., 2005. Toward a Neoproterozoic composite carbon-isotope record. Geol. Soc. Am. Bull. 117, 1181–1207. doi:10.1130/B25630.1.
Hambrey, M.J., 1982. Late Precambrian diamictites of northeastern Svalbard. Geol. Mag. 119, 527–551.
Hambrey, M.J., Harland, W.B., 1981. Earth's pre-Pleistocene glacial record. Cambridge University Press, London. 1004 pp.
Hambrey, M.J., Spencer, A.M., 1987. Late Precambrian glaciation of central East Greenland. Meddr Grønland Geosci. 19 50 pp.
Harland, W.B., 1964. Evidence of late Precambrian glaciation and its significance. In: Nairn, A.E.M. (Ed.), Problems in Palaeoclimatology. Interscience, London, pp. 119–149.
Higgins, J.A., Schrag, D.P., 2003. Aftermath of a snowball Earth. Geophys. Geochem. Geosyst. 4. doi:10.1029/2002GC000403.
Hildebrand, R.S., 2009. Did westward subduction cause Cretaceous–Tertiary orogeny in the North American Cordillera? Geol. Soc. Am. Sp. Pap. 457 71 pp.
Hoffman, P.F., 2005. 28th DeBeers Alex. Du Toit Memorial Lecture: On Cryogenian (Neoproterozoic) ice-sheet dynamics and the limitations of the glacial sedimentary record. S. Afr. J. Geol. 108, 557–576.
Hoffman, P.F., 2010. Strange bedfellows: glacial diamictite and cap carbonate from the Marinoan (635 Ma) glaciation in Namibia. Sedimentology Special Decadal Issue.
Hoffman, P.F., Halverson, G.P., 2008. Otavi Group of the western Northern Platform, the Eastern Kaoko Zone and the western Northern Margin Zone. In: Miller, R.McG. (Ed.), The Geology of Namibia. Handbook of the Geological Survey of Namibia, Windhoek, vol. 2. 13.69–13.136.
Hoffman, P.F., Li, Z.X., 2009. A palaeogeographic context for Neoproterozoic glaciation. Palaeogeogr. Palaeoclimatol. Palaeoecol. 277, 158–172.
Hoffman, P.F., Schrag, D.P., 2002. The snowball Earth hypothesis: testing the limits of global change. Terra Nova 14, 129–155.
Hoffman, P.F., Kaufman, J.A., Halverson, G.P., 1998. Comings and goings of global glaciations on a Neoproterozoic carbonate platform in Namibia. GSA Today 8, 1–9.

Hoffman, P.F., Halverson, G.P., Domack, E.W., Husson, J.M., Higgins, J.A., Schrag, D.P., 2007. Are basal Ediacaran (635 Ma) post-glacial "cap dolostones" diachronous? Earth Planet. Sci. Lett. 258, 114–131.
Hoffmann, K.-H., Prave, A.R., 1996. A preliminary note on a revised subdivision and regional correlation of the Otavi Group based on glaciogenic diamictites and associated cap dolomites. Communs Geol. Surv. Namibia 11, 77–82.
Hoffmann, K.-H., Condon, D.J., Bowring, S.A., Crowley, J.L., 2004. U–Pb zircon date from the Neoproterozoic Ghaub Formation, Namibia: constraints on Marinoan glaciation. Geology 32, 817–820. doi:10.1130/G20519.l.
Hyde, W.T., Crowley, T.J., Baum, S.K., Peltier, W.R., 2000. Neoproterozoic 'snowball Earth' simulations with a coupled climate/ice-sheet model. Nature 405, 425–429.
James, N.P., Narbonne, G.M., Kyser, T.K., 2001. Late Neoproterozoic cap carbonates: Mackenzie Mountains, northwestern Canada: precipitation and global glacial meltdown. Can. J. Earth Sci. 38, 1229–1262.
Jamieson, T.F., 1882. On the cause of the depression and re-elevation of the land during the glacial period. Geol. Mag. 9 (400–407), 457–466.
Jiang, G., Kennedy, M.J., Christie-Blick, N., 2003. Stable isotopic evidence for methane seeps in Neoproterozoic postglacial cap carbonates. Nature 426, 822–826.
Jiang, G., Kennedy, M.J., Christie-Blick, N., Wu, H., Zhang, S., 2006. Stratigraphy, sedimentary structures, and textures of the late Neoproterozoic Doushantuo cap carbonate in South China. J. Sed. Res. 76, 978–995.
Kauffman, E.G., Arthur, M.A., Howe, B., Scholle, P.A., 1996. Widespread venting of methane-rich fluids in Late Cretaceous (Campanian) submarine springs (Tepee Buttes), Western Interior seaway, U.S.A. Geology 24, 799–802.
Kellerhals, P., Matter, A., 2003. Facies analysis of a glaciomarine sequence, the Neoproterozoic Mirbat Sandstone Formation, Sultanate of Oman. Eclogae Geol. Helv. 96, 49–70.
Kendall, C.G., St, C., Warren, J., 1987. A review of the origin and setting of tepees and their associated fabrics. Sedimentology 34, 1007–1027.
Kennedy, M.J., 1996. Stratigraphy, sedimentology, and isotopic geochemistry of Australian Neoproterozoic postglacial cap dolostones: deglaciation, $\delta^{13}C$ excursions, and carbonate precipitation. J. Sed. Res. 66, 1050–1064.
Kennedy, M.J., Runnegar, B., Prave, A.R., Hoffmann, K.-H., Arthur, M.A., 1998. Two or four Neoproterozoic glaciations? Geology 26, 1059–1063.
Kennedy, M.J., Christie-Blick, N., Sohl, L.E., 2001. Are Proterozoic cap carbonates and isotopic excursions a record of gas hydrate destabilization following Earth's coldest intervals? Geology 29, 443–446.
Lewis, J.P., Weaver, A.J., Eby, M., 2007. Snowball versus slushball Earth: dynamic versus nondynamic sea ice? J. Geophys. Res. 112, C11014. doi:10.1029/2006JC004037.
Li, Z.X., Bogdanova, S.V., Collins, A.S., Davidson, A., De Waele, B., Ernst, R.E., Fitzsimons, I. C.W., Fuck, R.A., Gladkochub, D.P., Jacobs, J., Karlstrom, K.E., Lu, S., Natapov, L.M., Pease, V., Pisarevsky, S.A., Thrane, K., Vernikovsky, V., 2008. Assembly, configuration, and break-up history of Rodinia: a synthesis. Precambrian Res. 160, 179–210.
Liu, Y., Peltier, W.R., 2010. A carbon cycle coupled climate model of Neoproterozoic glaciation: influence of continental configuration on the formation of a "soft snowball". J. Geophys. Res. 115, D17111. doi:10.1029/2009JD013082.
Lythe, M.B., Vaughan, D.G., BEDMAP Consortium, 2001. BEDMAP: a new ice thickness and subglacial topographic model of Antarctica. J. Geophys. Res. B6, 11,335–11,351.
Macdonald, F.A., Strauss, J.V., Rose, C.V., Schrag, D.P., in press. Sturtian age iron formation on the Kalahari Craton and implications for the oxidation of Neoproterozoic oceans. Am. J. Sci.
McCay, G.A., Prave, A.R., Alsop, G.I., Fallick, A.E., 2006. Glacial trinity: Neoproterozoic Earth history within the British–Irish Caledonides. Geology 34, 909–912. doi:10.1130/G22694A.1.
McMechan, M.E., 2000. Vreeland diamictites–Neoproterozoic glaciogenic slope deposits, Rocky Mountains, northeast British Columbia. Bull. Can. Petrol. Geol. 48, 246–261.
Michaelis, W., Seifert, R., Nauhaus, K., Treude, T., Thiel, V., Blumenberg, M., Knittel, K., Gieseke, A., Peterknecht, K., Pape, T., Boetius, A., Amann, R., Jørgensen, B.B., Widdel, F., Peckmann, J., Pimenov, N.V., Gulin, M.B., 2002. Microbial reefs in the Black Sea fueled by anaerobic oxidation of methane. Science 297, 1013–1015.
Nédélec, A., Affaton, P., France-Lanord, C., Charrière, A., Alvaro, J., 2007. Sedimentology and chemostratigraphy of the Bwipe Neoproterozoic cap dolostones (Ghana, Volta Basin): a record of microbial activity in a peritidal environment. C.R. Geosci. 339, 223–239.
Nogueira, A.C.R., Riccomini, C., Sial, A.N., Moura, C.A.V., Fairchild, T.R., 2003. Soft-sediment deformation at the base of the Neoproterozoic Puga cap carbonate (southwestern Amazon craton, Brazil): confirmation of rapid icehouse to greenhouse transition in snowball Earth. Geology 31, 613–616.
Pattyn, F., 2010. Antarctic conditions inferred from a hybrid ice sheet/ice stream model. Earth Planet. Sci. Lett. 295, 451–461.
Penck, A., 1882. Schwankungen des Meerespiegels (Fluctuations in sea-level). Jahrb. Geograph. Gesell. München 7.
Plummer, P.S., 1978. Note on the palaeoenvironmental significance of the Nuccaleena Formation (upper Precambrian), central Flinders Ranges, South Australia. J. Geol. Soc. Aust. 25, 395–402.
Pollard, D., Kasting, J.F., 2004. Climate-ice sheet simulations of Neoproterozoic glaciation before and after collapse to Snowball Earth. In: Jenkins, G.S., McMenamin, M.A.S., McKay, C.P., Sohl, L. (Eds.), The Extreme Proterozoic: Geology, Geochemistry, and Climate. : Geophys. Monogr., 146. American Geophysical Union, Washington, DC, pp. 91–105.
Pollard, D., Kasting, J.F., 2005. Snowball Earth: a thin-ice solution with flowing glaciers. J. Geophys. Res. 110, C07010. doi:10.1029/2004JC002525.
Raub, T.D., Evans, D.A.D., 2006. Magnetic reversals in basal Ediacaran cap carbonates: a critical review. EOS Trans. Am. Geophys. Union 87 (36) Joint Assembly Suppl. Abstr. GP41-02.
Rieu, R., Allen, P.A., Plötze, M., Pettke, T., 2007. Climatic cycles during a Neoproterozoic "snowball" glacial epoch. Geology 35, 299–302.
Rose, C.V., Maloof, A.C., 2010. Testing models for post-glacial 'dap dolostone' deposition: Nuccaleena Formation, South Australia. Earth Planet. Sci. Lett. 296, 165–180.
Shields, G.A., 2005. Neoproterozoic cap carbonates: a critical appraisal of existing models and the plumeworld hypothesis. Terra Nova 17, 299–310.
Shields, G.A., Deynoux, M., Strauss, H., Paquet, H., Nahon, D., 2007. Barite-bearing cap dolostone of the Taoudéni Basin, northwest Africa: sedimentary and isotopic evidence for methane seepage after a Neoproterozoic glaciation. Precambrian Res. 154, 209–235.
Stowe, C.W., Hartnady, C.J.N., Joubert, P., 1984. Proterozoic tectonic provinces of Southern Africa. Precambrian Res. 25, 229–231.
Sumner, D.Y., 2002. Decimetre-thick encrustations of calcite and aragonite on the sea-floor and implications for Neoarchaean and Neoproterozoic ocean chemistry. Spec. Pub. Int. Ass. Sediment. 33, 107–120.
Tankard, A.J., Jackson, M.P.A., Eriksson, K.A., Hobday, D.K., Hunter, D.R., Minter, W.E.L., 1982. Crustal Evolution of Southern Africa. Springer-Verlag, New York. 523 pp.
Tanner, W.F., Clark, J.A., 1976. Greenland's rapid postglacial emergence: a result of ice–water gravitational attraction: comment and reply. Geology 4, 797–798.
Tapscott, C., Clark, J.A., 1976. Greenland's rapid postglacial emergence: a result of ice–water gravitational attraction: comment and reply. Geology 4, 452–454.
Trindade, R.I.F., Macouin, M., 2007. Paleolatitude of glacial deposits and paleogeography of Neoproterozoic ice ages. C.R. Geosci. 339, 200–211.
Trindade, R.I.F., Font, E., D'Agrella-Filho, M.S., Nogueira, A.C.R., Riccomini, C., 2003. Low-latitude and multiple geomagnetic reversals in the Neoproterozoic Puga cap carbonate, Amazon craton. Terra Nova 15, 441–446.
Van Dijke, J.J., Veldkamp, A., 1996. Climate-controlled glacial erosion in the unconsolidated sediments of northwestern Europe, based on a genetic model for tunnel valley formation. Earth Surf. Process. Land. 21, 327–340.
Wallace, J.M., Hobbs, P.V., 1977. Atmospheric Science: An Introductory Survey. Academic Press, San Diego. 467 pp.
Wang, J., Jiang, G., Xiao, S., Li, Q., Wei, Q., 2008. Carbon isotope evidence for widespread methane seeps in the ca 635 Ma Doushantuo cap carbonate in South China. Geology 36, 347–350.
Warren, S.G., Brandt, R.E., Grenfell, T.C., McKay, C.P., 2002. Snowball Earth: ice thickness on the tropical ocean. J. Geophys. Res. 107. doi:10.1029/2001JC001123.
Xiao, S., Bao, H., Wang, H., Kaufman, A.J., Zhou, C., Li, G., Yuan, X., Ling, H., 2004. The Neoproterozoic Quruqtagh Group in eastern Chinese Tianshan: evidence for a post-Marinoan glaciation. Precambrian Res. 130, 1–26.
Zhou, C., Peng, H., Yan, X., 2010. Timing the deposition of ^{17}O-depleted barite at the aftermath of Nantuo glacial meltdown in South China. Geology 38, 903–906.